Accepted Manuscript

Title: Synthesis and adsorption behavior of mesoporous alumina and Fe-doped alumina for the removal of dominant arsenic species in contaminated waters

Authors: N. Inchaurrondo, C. di Luca, F. Mori, A. Pintar, G. Žerjav, M. Valiente, C. Palet

PII: S2213-3437(19)30024-7
DOI: https://doi.org/10.1016/j.jece.2019.102901
Article Number: 102901

Reference: JECE 102901

To appear in:

Received date: 11 September 2018
Revised date: 27 November 2018
Accepted date: 10 January 2019

Please cite this article as: Inchaurrondo N, di Luca C, Mori F, Pintar A, Žerjav G, Valiente M, Palet C, Synthesis and adsorption behavior of mesoporous alumina and Fe-doped alumina for the removal of dominant arsenic species in contaminated waters, *Journal of Environmental Chemical Engineering* (2019), https://doi.org/10.1016/j.jece.2019.102901

Synthesis and adsorption behavior of mesoporous alumina and Fe-doped alumina for the removal of dominant arsenic species in contaminated waters

N. Inchaurrondo[*1], C. di Luca[1], F. Mori[2], A. Pintar[3], G. Žerjav[3], M. Valiente[4], C. Palet[4]

[1]Department of Chemical Engineering. Institute of Materials Science and Technology (INTEMA), University of Mar del Plata and National Research Council (CONICET), Av. J. B. Justo 4302, 7600 Mar del Plata, Argentina.

[2]FIQ-UNL, INCAPE-CONICET, Santiago del Estero 2829, S3000AOM Santa Fe, Argentina.

[3]Department for Environmental Sciences and Engineering, National Institute of Chemistry, Hajdrihova 19, SI-1001 Ljubljana, Slovenia.

[4]Centre Grup de Tècniques de Separació en Química, Departament of Chemistry, Universitat Autònoma de Barcelona, 08193 Barcelona, Catalunya, Spain.

* Correspondence to: ninchaurrondo@gmail.com.

Graphical abstract

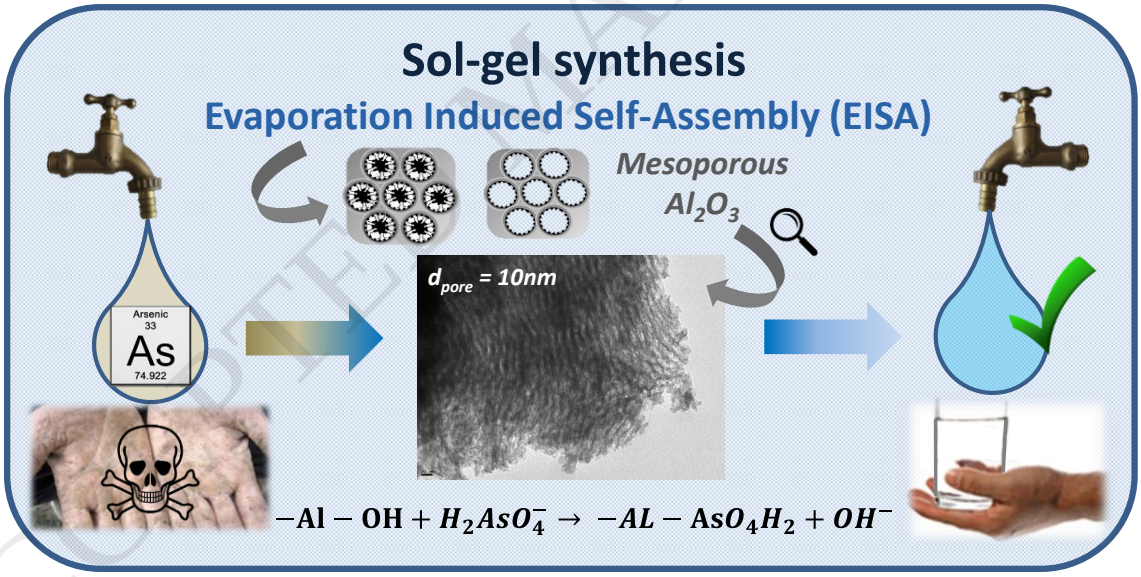

Highlights

- Mesoporous Al_2O_3 and Fe-Al_2O_3 were synthesized by a sol-gel methodology.
- Mesoporous synthesized materials were effective As(III) and As(V) adsorbents.
- Mesoporous alumina showed better performance than commercial alumina.

- Well-defined channeled mesostructures avoided pore blockage, facilitating adsorption.
- Arsenic uptake may occur through ligand exchange and electrostatic interaction.

Abstract

Ordered mesoporous Al_2O_3 and Fe-Al_2O_3 materials were synthesized at room temperature by an easy and environmentally friendly self-assembly sol-gel route, to be tested for arsenic removal.

Solid samples were thoroughly characterized by several techniques. Synthetized and commercial alumina samples were evaluated as adsorbents for the removal of dominant arsenic species under a wide pH range (3.6-11.5). The mesoporous alumina showed higher adsorption capacity (90 mg/g As(V), pH_{eq} 4) than commercial alumina (54 mg/g As(V), pH_{eq} 4), due to its amorphous structure, uniform accessible mesopores and higher surface acidity. The Fe bearing material exhibited strong As affinity.

As(III) adsorption resulted much lower than for arsenate (maximum uptake of 16 mg/g, at pH 8), since As(III)-adsorbent interaction is only based on weak Van der Waals force. Arsenic isotherms adjusted well to the Freundlich model and more accurately to the three parameters Sip´s model. The kinetics results fitted the Elovich model.

As pH increased, adsorption capacity decreased due to the reduction of electrostatic interactions. Under alkaline conditions arsenic desorption was achieved, although the stability of the material was compromised.

The presence of several interfering ions was evaluated. Phosphate ions showed the highest interference. The use of a tap water matrix increased As(V) adsorption, encouraging the use of these materials in the treatment of real polluted waters.

Key-words: mesoporous alumina, Fe doped alumina, As(III) and As(V) removal, adsorption mechanism.

1. Introduction

Arsenic contaminated waters are a matter of great concern in several areas of the world. The chronic exposure to this pollutant can lead to adverse health effects such as skin lesions and lung, bladder, and kidney cancer [1].

Arsenic is mobilized by natural weathering reactions, biological activity, geochemical reactions, volcanic emissions and some anthropogenic activities (use of fertilizers, pesticides, glass, ceramics, mining/smelting operations, petroleum refineries) [2-3]. Arsenic appears as inorganic as well as organic species; however, in an aqueous environment, inorganic arsenic species (arsenite, As(III), and arsenate, As(V)) are more abundant than organic ones. Arsenate dominates at high redox potentials and oxygen-rich aerobic environments, is less toxic than arsenite, but more abundant and mobile in natural surface waters; whereas, arsenite is found mostly in anaerobic environments such as groundwater [4].

In Argentina, arsenic contamination affects mainly urban and rural poor populations, not connected to drinking water networks [4]. Due to its high toxicity, the World Health Organization (WHO) recommends a limit of 10 ppb of arsenic in water for human consumption [1]. However, in Argentina, the regions with the highest arsenic content in water (Chaco-Pampean plain, Puna and Cuyo), show values between 4 and 5.3 mg/L (mainly As(V)). Also, a high arsenic content of 14.97 mg/L was reported in the province of Santiago del Estero [4]. In some places, 99% of groundwater exceeds the guideline of 10 ppb [4], therefore it is imperative to optimize an affordable and simple operation arsenic removal process.

Various technologies have been applied to solve this problem, such as co-precipitation, alum or iron coagulation, membrane filtration, bioremediation or adsorption [5]. Among these alternatives, the adsorption technology is very promising because of its simple operation, low cost, no chemical addition, regeneration capability and low energy consumption. The accessibility of the adsorption process allows its implementation in individual homes and small community systems and makes it ideal to implement in developing countries.

Several materials have been tested for arsenic removal such as activated carbon, mineral oxides, zeolites, polymer resin or biological materials [4, 6], with the purpose of finding a regenerable adsorbent with great removal capacity and stability. Activated alumina (AA) has received substantial attention due to its relatively high surface area and high affinity towards several inorganic anions [7-8]. Results presented by other authors, employing alumina or iron oxides, are collected and presented in Table 1, most of them only focused on As(V) removal.

In spite its benefits, conventional AA has poorly defined pore structures and low adsorption capacities. An ideal adsorbent is expected to have uniform accessible pores,

a three dimensional pore system, high surface area, fast adsorption kinetics and good physical and/or chemical stability [7]. Therefore, the use of mesoporous alumina (MA) has been proposed to improve the adsorption efficiency of AA due to its large surface area and narrow pore-size distribution, with uniform channels [23-26]. Moreover, they allow the incorporation of active species through different methodologies, obtaining functional materials with greater reactivity and selectivity [27].

Among different preparation methodologies, sol-gel is one of the most preferred methods for the synthesis of mesoporous metal oxides since it provides a low-temperature route with excellent control over mixing [28-29]. Based on the sol-gel methodology, a remarkable way of achieving the growth of ordered MA structures is the solvent Evaporation Induced Self-Assembly (EISA). This one-pot strategy consists in the self-assembly of a non-ionic triblock copolymer (P123), used as a structure directing agent, and the metal precursors, in an ethanolic solution with nitric acid [30]. The incorporation of metallic species into the host structure during the MA synthesis may result in a strong interaction between the doped metal and the alumina matrix, with the development of large uniform mesopores [31]. This enhances the accessibility to surface sites and allows a homogeneous distribution of active sites, with improved thermal stability [31].

Although, there are several studies dealing with arsenic adsorption by alumina materials, the improvements obtained from using MA, synthetized by the EISA methodology, have not been deeply studied. Hence, in this contribution, we present a simple and reproducible method to synthesize ordered mesoporous alumina, through an environmentally friendly sol-gel route with P123 as soft template, to be applied to the adsorption of As(V) and As(III) in contaminated waters. Moreover, there has been great interest in the use of bimetals and bimetal oxides for the removal of environmental contaminants with encouraging treatment efficiencies [10, 19, 32]. In particular, Fe based materials have shown higher affinity toward arsenate as compared to non-iron adsorbents [6, 15, 18, 32]. Thus, the addition of Fe during the MA synthesis was also studied. Subsequently, the performance of the synthesized materials was evaluated in the removal of As(V) and As(III) species, focusing on the equilibrium properties, isotherms and kinetics adsorption behavior, at different pH values. A comparison with a commercial gamma alumina was also carried out to assess the improvements obtained from the sol-gel synthesis. Additionally, the presence of interfering anions was also studied in order to evaluate a more realistic water matrix.

2. Methodology

2.1. Chemicals and reagents

Analytical-grade reagents were used as supplied without further purification. The reagents used in this work were: sodium acetate trihydrate (>99% ACS, Aldrich), acetic acid (>99% ACS, Aldrich), sodium hydrogen arsenate heptahydrate (Aldrich), sodium metaarsenite (98%, Aldrich), ammonium molybdate tetrahidrate (Fluka), sodium carbonate (99.5%, Acros organics), sodium chloride (Panreac), potassium nitrate (99%, Aldrich), sodium sulphate anhydrous (Sigma), sodium phosphate dibasic heptahydrate (Sigma), L(+) ascorbic acid (Scharlau), sulphuric acid (95-97%, Scharlau), aluminum isopropoxide (≥ 98%, Aldrich), ferric nitrate nonahydrate $Fe(NO_3)_3.9H_2O$ (AppliChem), nitric acid HNO_3 (70% wt./wt., Cicarelli PA), hydrochloric acid HCl (37% wt./wt., Merck), tri-block copolymer Pluronic P123 (Aldrich, symmetric tri-block copolymer constituted of poly(ethylene oxide) (PEO) and poly(propylene oxide) (PPO)), and anhydrous ethanol (99.5%, Cicarelli).

2.2. Synthesis of mesoporous alumina adsorbents

Alumina powders were synthesized by using an adaptation and scaling-up over the evaporation-induced self-assembly methodologies reported by Yuan and Morris separately [30]. During the synthesis, 20 g of tri-block copolymer Pluronic P123 was dissolved in 200 mL of anhydrous ethanol at room temperature and allowed to stir for 4 h (solution A). Meantime, solution B was prepared from 32 mL of nitric acid and 100 mL of anhydrous ethanol. An amount of 0.2 mol of aluminum isopropoxide was added to solution B under vigorous stirring. Once the synthesis precursors were dissolved, the two solutions were combined in one-pot and 100 mL of anhydrous ethanol was used to thoroughly transfer the aluminum isopropoxide solution. The final solution was continuously stirred for 5 h at room temperature. The molar ratio $[Al^{3+}]$:[P123]:[EtOH]:$[HNO_3]$ in the final solution was fixed at 1:0.017:30:2.5. In order to avoid the effect of humidity and to control the hydrolysis rate of the aluminum alkoxide, the synthesis was carried out inside a dry glove box under N_2 atmosphere. Afterwards, solvent evaporation of the homogeneous sol was performed in a drying oven at 60°C for 48 h (air atmosphere without stirring). The resulting xerogel was calcined in a muffle furnace with integrated air circulation by increasing temperature from room temperature to 400°C (heating rate of 1°C/min) and held at the final

temperature for 4 h. The calcined samples were ground in an agate mortar to reach the final mesoporous alumina powders, labeled as MA. The adsorption performance of the synthetized material was contrasted with the one of a commercial γ-Al_2O_3 (SASOL, 200 m^2/g), labeled as CA.

In addition, the alumina matrix was doped with iron to form the mesoporous Fe-alumina adsorbent. This material was prepared by adding a Fe precursor, ferric nitrate, to solution A. The other steps of the synthesis were the same as those given above. The total quantity of iron and aluminum was kept constant (0.2 mol) and the molar ratio [Fe]:[Al] was adjusted to 0.064. The total iron content of the Fe-doped adsorbent resulted in 4.7% wt./wt. (labeled as MA-5Fe).

2.3. Adsorbents characterization techniques

The characteristics of the alumina adsorbents were determined by different conventional techniques.

2.3.1. N_2 Physisorption

The nitrogen adsorption and desorption isotherms at -196 °C were measured using a Micrometrics ASAP-2020 instrument. Specific surface areas were calculated from the adsorption branches by the BET method, while pore size distribution were deduced from the desorption branches. Before analysis, each sample was degassed overnight at 120 °C under vacuum conditions.

2.3.2. X-Ray Diffraction (XRD)

Powder XRD measurements were obtained with a PANalytical X'Pert Pro diffractometer by using CuKα radiation (λ = 1.54056 Å). The diffractograms were recorded over $10° < 2\theta < 70°$ range and compared to the JCPDS files to confirm phase identities.

2.3.3. Transmission Electron Microscopy (TEM)

The microstructure of the alumina adsorbents was studied by TEM using a TEM JEOL 100 CX II instrument. Samples were prepared by dispersing the powdered catalysts in ethanol and dropping the suspension onto a standard formvar-coated copper grid.

2.3.4. Thermogravimetric Analysis (TGA)

TGA of the synthetized xerogels was performed with a TGA Q500 V 20.13 (TA instruments) thermobalance under air atmosphere at a heating rate of 10 °C/min and a temperature interval between 25 – 700 °C.

2.3.5. Point of Zero Charge (PZC)

The PZC was determined by means of mass titration method. Portions of solid samples (0.05 g) were added to a stirred aqueous solution with initial pH 6. The pH of the system changes gradually and approaches to a constant value, which equals to PZC. Measurements were performed at 25 ºC in 25 mL of 0.005 mol/L NaCl aqueous solutions, purged with 750 mL/min of N_2.

2.3.6. Temperature Programmed Desorption of Pyridine (TPD)

Acidic properties were determined by pyridine TPD as the probe molecule, using a Pyris 1 TGA instrument (Perkin Elmer). The adsorbent samples were pretreated by heating from 50 to 400 ºC (10 ºC/min, purged with air) and hold at 400 ºC for 15 min to eliminate surface impurities. Then the samples were cooled to 120 ºC and purged with N_2, followed by the surface saturation with pyridine until constant weight. The excess of probe molecule was then removed in N_2 flow (120 min). The pyridine covered samples were subjected to TG by heating up from 120 to 400 ºC (20 ºC/min).

2.3.7. Fourier-Transform Infrared Spectroscopy (FTIR)

Different species in the sample were identified by FTIR/attenuated total reflection spectroscopy (FTIR/ATR Nicolet 6700). Spectra were recorded in the region of 4000–400 cm^{-1}, at room temperature by performing 64 scans with a resolution of 2 cm^{-1}.

2.3.8. X-ray Photoelectron Spectroscopy (XPS)

XPS analyses were performed using a multi-technique system (SPECS) equipped with a dual Mg/Al X-ray source, and a hemispherical PHOIBOS 150 analyzer operating in the fixed analyzer transmission (FAT) mode. The spectra were obtained using an Al Kα radiation (h.ν = 1486.6 eV) operated at 200 W and 12 kV. The pass energy for the element scan was 30 eV. The working pressure in the analyzing chamber was less than 8×10^{-10} kPa. The spectra of As 3d, O 1s, C 1s, Fe 2p, Al 2p, Al 2s and Auger As peak regions were recorded for each sample. The data treatment was performed with the Casa XPS program (Casa Software Ltd, UK). The peak areas were determinate by integration employing a Shirley-type background. Peaks were considered a mixture of Gaussian and Lorentzian functions. For the quantification of the elements, we used the sensitivity factors provided by the manufacturer.

2.4. Analytical measurements

As(V) concentration was determined by the molybdene blue method at 855 nm, using UV-1800 spectrophotometer [33]. As(III), Fe and Al in the supernatant were determined by Inductively Coupled Plasma Mass Spectrometry, ICP-MS (XSERIES 2 ICP-MS, Thermo Scientific, USA).

Total Fe content of MA-5Fe solid sample was determined by a standard colorimetric test (FerroVer®Iron Reagent, HACH) over the digested solid samples in HNO_3−HF.

pH was monitored using a pH meter micropH 2002 (Crison instruments, S.A., Spain), with a combined glass electrode.

2.5. Adsorption experiments

Batch adsorption experiments were conducted to determine the As adsorption equilibrium properties of the studied materials, by using known amounts of such adsorbents with different arsenic solutions (40 mL), adjusted at different pH values, under constant stirring.

All the adsorption experiments were carried out at room temperature using polypropylene (PP) vessels on a rotary stirrer, during a maximum of 24 h (except for As(III) at initial pH of 11, where the experiment was extended up to 48 h). Stock solutions of 500 mg/L of As(V) and 100 mg/L of As(III) were prepared with Milli Q water and then diluted to various concentrations. The initial pH of arsenic solutions were adjusted as required with HNO_3 (0.1 M or 1 M), NaOH (0.1 M) to adjust at pH 11 or 0.02 M acetate buffer at pH 3.7.

The pH of the resulting suspensions was monitored throughout the course of adsorption experiments; the final pH measured at the end of the experiments is the value reported as equilibrium pH (pH_{eq}).

The adsorption capacity, Q_E (mg/L), of the adsorbent was calculated based on the following equation:

$$Q_E = (C_0 - C_E) * \frac{V}{m} \qquad (1)$$

where C_0 (mg/L) and C_E (mg/L) represent the initial and equilibrium arsenic concentrations, respectively, V (L) is the volume of the arsenic solution and m (g) is the mass of adsorbent.

2.5.1. Determination of adsorption isotherms

The arsenate and arsenite adsorption isotherms were obtained at different initial pH values (3.7, 7.5 and 11), by using adsorbent concentrations of 0.5 g/L (pH 3.7 and 7.5) and 5 g/L (pH 11).

To evaluate the isotherm, different arsenic concentrations were checked: 5, 10, 25, 50, 100, 250, 500 mg/L for As(V) and 5, 10, 25, 50, 100 mg/L for As(III).

2.5.2. Determination of kinetic curves

The kinetic curves for As(V) and As(III) were also obtained at different initial pH values (3.7, 7.5 and 11), by adding the same amounts of adsorbent as mentioned in section 2.5.1. The arsenic initial concentration was 100 mg/L for As(V) and 20 mg/L for As(III). Samples were collected at 0.5, 2, 5, 10, 24 h (and 48 h for As(III) at initial pH of 11).

2.5.3. Influence of interfering anions and water matrix

The Cl^- , SO_4^{2}, NO_3^-, PO_3^{3-} interference was checked using As(V) concentration of 20 mg/L, under pH 7.5 (near to real waters pH), with an adsorbent dose of 0.5 g/L and a molar ratio of [As]:[anion] = 1:25. In order to test a more realistic water matrix, the adsorption test was also carried out with an arsenate solution prepared with tap water, by using the same adsorbent load and initial As(V) concentration. The tap water sample was analyzed by Companyia d'Aigües de Sabadell S.A, revealing the presence of: Cl^- (90.4 mg/L), Na^- (37.4 mg/L), SO_4^{-2} (68.7 mg/L), $CaCO_3$ (174 mg/L).

2.5.4. Desorption of As(V)

Preliminary desorption experiments were performed by using samples obtained from adsorption tests with 5 g/L of MA and MA-5Fe, in 50 mg/L of As(V) aqueous solutions (Milli Q water, initial pH 7.5), stirred during 24 h. After the adsorption test, the samples were filtered and dried at room temperature during 48 h, and then at 50 ºC for 24 h. To perform the As(V) desorption tests, mass samples of 0.05 g were stirred during 5 hours in 25 mL solutions of different initial pH values: HNO_3 (0.01 M, pH 1.9), Milli Q water pH 8, NaOH (0.01 M, pH 11.5) and NaOH (0.05 M, pH 12).

2.6. Isotherm models and kinetics parameters

The adsorption results were fitted by using Langmuir, Freundlich, Temkin, Dubinin–Radushkevich and Sip´s isotherm models.

2.6.1. Langmuir isotherm

The Langmuir equation (Eq. 2) assumes: (1) fixed number of accessible sites with the same energy, available on the adsorbent surface; (2) reversible adsorption; (3) once an adsorbate occupies a site, no further adsorption can occur on that site; and (4) there is no interaction between adsorbate species [34].

$$q_e = \frac{Q_m * K_L * C_e}{1 + K_L * C_e} \qquad (2)$$

Q_m (mg/g) is the maximum saturated monolayer adsorption capacity of an adsorbent and K_L (L/mg) is a constant related to the affinity between an adsorbent and adsorbate. Good

adsorbents present high theoretical adsorption capacity Q_m and a steep initial sorption isotherm slope (high K_L) [34].

2.6.2. Freundlich isotherm

The Freundlich isotherm (Eq. 3) is the earliest known relationship describing the non-ideal and reversible adsorption, not restricted to the formation of a monolayer. This empirical model can be applied to multilayer adsorption, with non-uniform distribution of adsorption heat and affinities over the heterogeneous surface [35].

$$q_e = K_F * C_e{}^n \qquad (3)$$

The adsorption coefficient, K_F, characterizes the strength of adsorption. The higher the value of K_F is, the higher is the adsorbent loading to be achieved. The exponent n is related to the energetic heterogeneity of the adsorbent surface, determines the curvature of the isotherm and speed of saturation. Freundlich isotherms with $n < 1$ show relative high adsorbent loadings at low adsorbate concentrations. Therefore, they are referred to as favorable isotherms, whereas isotherms with $n > 1$ are characterized as unfavorable ones [36].

2.6.3. Dubinin–Radushkevich (DR) isotherm

The DR isotherm (Eqs. 4 and 5), is an empirical model initially conceived for the adsorption of subcritical vapors onto micropore solids following a pore filling mechanism [35]. The model has successfully fitted high solute activities and intermediate range of concentrations data, but has unsatisfactory asymptotic properties and does not predict the Henry's law at low pressure [35].

The mathematical expression for DR equation in the liquid phase system is:

$$q_e = Q_{DR} * e^{-K_{RD}*\varepsilon^2} \qquad (4)$$

$$\varepsilon = R * T * \ln(1 + \frac{1}{C_e}) \qquad (5)$$

where R and T represent the gas constant (8.314 J/mol K) and absolute temperature (K), respectively. The Q_{RD} (mg/g) is the maximum theoretical adsorption capacity, K_{RD} ($mol^2\ J^{-2}$) is a constant related to the sorption energy and ε is the Polanyi potential.

2.6.4. Temkin isotherm

The Temkin isotherm equation (Eq. 6) assumes that the heat of adsorption of all the molecules in the layer decreases linearly with coverage due to adsorbent–adsorbate interactions, and that the adsorption is characterized by a uniform distribution of the binding energies, up to some maximum binding energy [35]. The Temkin model is given by

$$q_e = \frac{R*T}{B} * \ln(A * C_e) \qquad (6)$$

Where R is the gas constant (8.314 J/mol K), T the temperature (K), B = ($-\Delta H$) the variation of adsorption energy (kJ mol^{-1}), and A is the Temkin equilibrium constant (L mg^{-1}).

The Temkin equation is superior in the prediction of gas phase equilibria, but adsorption in the liquid phase is a more complex phenomenon. Numerous factors including pH, solubility of the adsorbate in the solvent and surface chemistry of the adsorbent, influence the adsorption from liquid phase [37].

2.6.5. Sip´s model

Frequently, adsorption isotherms measured over broad adsorbate concentration ranges cannot be described exactly with only a single set of isotherm parameters or a single model adjustment. If the simple two-parameter isotherms should be maintained, different parameter sets have to be applied for different concentration ranges; otherwise the application of three-parameter isotherms is recommended [36]. The Sip´s model (Eq. 7) is another empirical model that can simulate both Langmuir and Freundlich behaviors [36]. This equation describes the saturation phenomenon at higher concentrations and at lower concentrations it reduces to the Freundlich isotherm [36].

$$q_e = \frac{Q_a*(K_a*C_e)^u}{1+(K_a*C_e)^u} \qquad (7)$$

Q_a is the maximum theoretical adsorption capacity of the system (mg/g); K_a is the affinity constant for adsorption (L/mg) and u is the index of heterogeneity.

The Sip´s isotherm uses a single value to describe the maximum adsorption capacity and does not require fitted adsorption capacity values at different pH values. Instead the affinity constant (K_a) can be varied to account for pH dependent sorption effects [38]. Since the heterogeneity index (u) is a material property, its value was assumed to be a constant at all pH values.

2.6.6. Assessment of kinetic parameters

To evaluate the sorption rates, empirical pseudo-first order (Eq. 8), pseudo-second order (Eq. 9), Elovich (Eq. 10) and the simplified Intra-particle diffusion model (Eq. 11) equations were adopted to model the experimental data.

$$\frac{dq_t}{dt} = k_1 * (q_e - q_t) \qquad (8)$$

$$\frac{dq_t}{dt} = k_2 * (q_e - q_t)^2 \qquad (9)$$

$$q_t = \frac{1}{\beta} * \ln(1 + \alpha * \beta * t) \qquad (10)$$

$$q_t = k_p * t^{0.5} + C \qquad (11)$$

The parameters k_1 (1/min) and k_2 (g mg^{-1} min^{-1}) are the pseudo-first order and the pseudo-second order rate constants, respectively; q_t and q_e are the arsenic adsorption amount (mg/g) at any time (t (min)) and at equilibrium, respectively.

The Elovich coefficients, α and β, represent the initial adsorption rate (g mg^{-1}min^{-2}) and the desorption coefficient (mg g^{-1}min^{-1}), respectively. The Elovich equation can be derived from either a diffusion-controlled process or a reaction-controlled process [39]

In the intra-particle diffusion model, *kp* (mg g^{-1} min^{-1}) is the rate constant and *C* (mg/g) is a constant associated with the thickness of the boundary layer, where a higher value of *C* corresponds to a greater effect on the limiting boundary layer [40]. If a plot of q_t against $t^{0.5}$ is linear and passes through the origin, the adsorption is entirely governed by intra-particle diffusion. In contrast, if the intra-particle diffusion plot gives multiple linear regions, then the adsorption process is controlled by a multistep mechanism. Therefore, a nonlinear run of the q–t$^{0.5}$ plot over a broad time interval is not evidence for missing intra-particle diffusion impact on adsorption kinetics [36].

The isotherm and kinetics parameters were obtained with the nonlinear method using the "*Solver add-in*" in Microsoft Office Excel. Several error functions were calculated such as the hybrid fractional error function (HYBRID) (Eq. 12), the average relative error (ARE) (Eq. 13) and the sum of the errors squared (ERRSQ), to predict the optimum isotherm model [35].

$$\frac{100}{m-p} * \sum \frac{(q_{e\ isotherm} - q_{e\ calc})^2}{q_{e\ isotherm}} \qquad (12)$$

$$\frac{100}{m} * \sum \left| \frac{q_{e\ isotherm} - q_{e\ calc}}{q_{e\ isotherm}} \right| \qquad (13)$$

$$\sum (q_{e\ isotherm} - q_{e\ calc})^2 \qquad (14)$$

Where *m* is the number of experimental points, *p* the number of parameters to be determined, $q_{e\ isotherm}$ is the experimental value and $q_{e\ calc}$ is the value calculated using the model.

3. Results

3.1 Adsorbents characterization

After thermal treatment at 400 ºC, TGA analysis confirmed that all organic residues from previous preparation steps were removed from the MA samples (see Fig. 1). TGA curves displayed three stages of weight loss, at different temperatures (Fig. 1). The total weight losses for the MA and MA-5Fe samples were c.a. 80%. The first step, the weight loss below 150 ºC, is attributable to the removal of physically adsorbed species, such as

water. The second step, located in the 150-225 ºC range, corresponds to the decomposition of the P123 template. Finally, the third step represents the remaining weight loss in the 225-500 ºC range, which is assigned to the dehydroxylation of OH-groups and conversion of hydrated alumina into transitional alumina [31].

The powdered MA and MA-5Fe materials calcined at 400 ºC were amorphous and no crystalline phases were detected by XRD (Fig. 2).

TEM images showed the development of ordered mesoporous structures with narrow channels of ca. 10nm (Fig. 3). For comparison purposes, Fig. 3 also shows the micrograph of a commercial gamma-alumina sample (CA), exposing significant differences on the alumina microstructure which can influence the accessibility of the arsenic adsorbates.

In agreement with TEM results, N_2 Physisorption measurements revealed the development of mesoporous materials with a BET surface area of 221 m^2/g for MA and 104 m^2/g for MA-5Fe. Both samples displayed type IV isotherms and H3 hysteresis loops, typical from mesoporous materials [41] and a narrow pore size distribution centered on 10 nm (Table 2 and Fig. 4). However, it should be noted that the Fe-doping and/or the scaling-up of the EISA methodology impacted negatively on the MA-5Fe porosity, showing a noticeable decrease on the specific surface area and the pore volume. Table 2 and Figure 4 also show the CA sample characterization results. The commercial alumina exhibited a BET surface area and pore volume of 200 m^2/g and 0.5 cm^3/g, respectively, with an average pore width of 7.15 nm. These values were slightly lower than the obtained for the MA adsorbent.

The CA physisorption isotherm displayed a different shape of pore structure, type IV with H2(b) hysteresis loop, which might indicate more complex pore structures in which network effects are important and can be related with pore blocking [41].

Surface reactivity is determined by the structural and coordinative arrangements around the surface metal centers. The point of zero charge (PZC) is a central concept in the adsorption of charged species and its position defines the affinity of the solid surface to the ionic species [42]. The PZC represents the pH at which the number of positively charges species ($M–OH_2^+$) equals the number of negatively charged species ($M–O^-$) nulling the net surface charge, where M stands for a surface metal center. The value of point of zero charge resulted in 7.5 for all samples, which is consistent with those reported in the literature for similar metal oxide systems [42]. This result means that

adsorbents surface might be positively charged and will adsorb/attract anions and/or negatively charged ligands from waters when working at pH < PZC.

Metal oxides reactivity is determined by its acidity and basicity. Hydroxyl groups formed at the surface behave as Brönsted acid sites, whereas Lewis acids and Lewis bases are sites located on metallic cations and coordinately unsaturated oxygens, respectively [8]. The acidity of mesoporous alumina samples was determined by TPD of pyridine (Table 3). The measurements revealed that Fe incorporation during the sol-gel synthesis of alumina (MA-5Fe) increased the quantity and density of acid sites in relation with MA. By contrast, the CA sample showed a lower concentration of surface acidic sites which might influence the uptake of arsenic species. All samples desorbed pyridine at around 235 ºC, which implies the same strength of acid sites.

3.2 Arsenic adsorption tests

3.2.1 pH effect

As(V) and As(III) maximum adsorption capacities under the tested conditions are presented in Table 4. Initial pH values of 3.7, 7.5 and 11.5 led to final equilibrium values of 4, 8 and 10, respectively. The mesoporous alumina presents high alkalinity or internal buffer capacity, which helps to maintain small pH changes [43]. As(V) isotherms at equilibrium pH values of 4, 8 and 10 are presented in Figures 5a,b,c,d for MA and MA-5Fe samples.

The three materials studied presented a PZC around 7.5 (see Table 2). The interaction between arsenic and the adsorbents depends not only on the surface charge but also in the speciation of the arsenic molecules. The equilibrium dissociation constants of the two arsenic oxidation states are quite different: H_3AsO_4 (As (V)) pKa_1= 2.19, pKa_2= 6.94, pKa_3= 11.5, and H_3AsO_3 (As(III)) pKa_1= 9.20, pKa_2= 12.1, pKa_3= 13.4.

During adsorption tests performed with initial pH 3.7 and 7.5, the predominant As(V) solution species remained negatively charged ($H_2AsO_4^-$ and or $HAsO_4^{2-}$). In that pH range, the surface charge of the materials was positive to neutral. Therefore, the adsorption of As(V) species occurred mostly via electrostatic interactions or ligand exchange. Lower pH favors the ligand exchange reaction since H_2O is easier to displace from metal biding sites than OH^- [44]. As it was mentioned before, the pH values increased after As(V) adsorption, under acidic and near-neutral media. This could be related to a protonation of the adsorbent surface and also to the ligand exchange reaction with either $H_2AsO_4^-$ or $HAsO_4^-$, accompanied by a release of OH^-.

As the initial pH increased from 3.7 to 7.5, the adsorption capacity decreased due to the reduction of the electrostatic interaction. Also, as pH increases, mono-charged $H_2AsO_4^-$ anions deprotonate to form double charged $HAsO_4^{2-}$ anions. If the ion exchange process is involved, the double-charged anions may require more functional sites, resulting in less arsenic adsorption.

Once pH>>PZC, the As(V) adsorption decreases much further, due to the Columbic inhibition between the negatively charged surface and the anionic species. In this pH range the As(V) adsorption may occur via H-bonding between the negative surface and $HAsO_4^{2-}$, competing with OH−. Also, even if a surface has a net negative charge, enough residual positive surface charges might still be present to attract some arsenic oxyanions.

As(III) isotherms at the equilibrium pH 8 and 10 are presented in Figures 6a,b for MA and MA-5Fe samples. Under pH 9.2 (first pKa of arsenite), the non-ionic H_3AsO_3 is the dominant arsenite specie and therefore the interaction is only based on weak van der Waals forces. Hence, at initial pH 3.7, the arsenite adsorption resulted negligible and in general adsorption uptakes of As(III) were much lower than the obtained for As(V). Several studies reported an optimum arsenite removal between pH 6 to 9 [2]; while higher pH values might cause a decline in arsenite uptake due to electrostatic repulsion. Despite this, high arsenite removal was observed at pH 10 for MA-5Fe. A possible explanation might be the dissolution of the material under alkaline media and posterior co-precipitation of arsenic species with Fe oxy-hydroxides (see section 3.2.5) [6, 45-46].

Taking into account that the affinity towards As(III) resulted lower than the affinity shown for As(V), it is highly recommendable to pre-oxidize the contaminant (Fenton reaction, ozonation, etc.) to maximize the removal efficiency of the total amount of arsenic from contaminated water samples [6].

3.2.2 Isotherms and adsorption kinetics

The As(V) isotherms parameters are presented in Table 5. According to these results, the Temkin model only described properly the arsenate adsorption under acidic pH. The variation of the adsorption energy, $B = (-\Delta H)$, resulted positive for all the studied materials, which indicates that the adsorption reaction is exothermic. On the other hand, the fitted Freundlich parameters described more effectively the arsenate adsorption behavior over the whole pH range, as seen by other authors [3, 7, 14, 23, 43].

The Freundlich constant per gram of adsorbent (K_F $mg^{n-1}*L^n/g$) was higher in the case of MA sample, which might be connected to its greater surface area in contrast to the MA-5Fe sample. However, MA and CA samples have comparable surface areas, therefore the increased adsorption capacity of the mesoporous alumina may be due to its particular structure and surface features, such as amorphous nature and higher concentration of Brönsted sites. As described previously in section 2.2, the MA sample was synthesized under conditions which minimized the formation of crystalline well-ordered surfaces, obtaining a high surface density of edge Al-OH groups [47]. Despite the similar pore diameters and surface areas in both adsorbents, the well-defined channels of P123-templated mesostructures, might prevent pore blockage while facilitating the access of metal ions to the adsorption sites [10, 48].

Another interesting tool of analysis is the arsenic uptake related to the specific surface area of each adsorbent. The Freundlich constant per square meter of surface area ($K´_F$ $mg^{n-1}*L^n/m^2$) was higher for the Fe-doped alumina, especially at acidic pH. While at neutral/alkaline pH, the $K´_F$ ($mg^{n-1}*L^n/m^2$) for MA and MA-5Fe resulted similar. According to these results, at pH < PZC arsenate species show increased affinity towards Fe sites, as observed by other authors [6, 15, 18, 32]. Taking into account characterization results, the increased arsenate uptake might be also associated with a higher density of acid sites in contrast to MA and CA samples (Table 2).

For all the studied materials, the *n* values obtained were similar and below the unity, which indicates favorable isotherms.

Table 6 shows the calculated Sip´s parameters for As(V) adsorption adjustment. In agreement with the other fitted isotherms, the maximum Q_a (mg/g) obtained was shown by the sample MA. The adsorption capacity (mg/g) of this sample was much higher than the value reached by the commercial alumina (CA) or the MA-5Fe sample. Again, the $Q´_a$ per square meter of surface area (mg/m^2) resulted maximum for the MA-5Fe sample and MA sample displayed higher $Q´_a$ than the commercial alumina. Consequently, as was discussed previously, the larger adsorption capacity shown by the synthesized alumina material (MA) would be mostly related to its amorphous structure, higher concentration of acid sites and the development of well-defined mesopores [10, 49, 47-48].

The values of the adsorption affinity constant (K_a) increased at acidic pH due to an enhancement of the electrostatic attraction between the adsorbent surface and the arsenate species (higher adsorption affinity).

The *u* values obtained for the alumina systems (MA, CA) were similar (around 0.44). While for the MA-5Fe sample resulted slightly lower (u = 0.35). As mentioned before for Freundlich isotherm, exponent values below the unity provide information about the favorability of As(V) adsorption onto the materials tested.

Table 7 shows As(III) isotherms parameters for the sol-gel synthetized materials. In this case, the Freundlich isotherm described properly the adsorption behavior at pH 8 and the DR model correlated better the arsenite removal, at pH 10. In general, the parameters obtained for both adsorbents (MA and MA-5Fe) resulted quite similar and slightly better for the MA-5Fe sample.

In the case of As(III), Sip´s equation was not applicable, since there was no agreement between the experimental and calculated adsorption capacities.

Kinetics studies were performed and the adsorption systems approach equilibrium after 5, 10 and 24 h, at equilibrium pH values of 4, 8 and 10, respectively. As was previously commented, at higher pH, the electrostatic attraction diminishes and the adsorption process slows down.

Table 8 and 9 present the kinetic parameters obtained. From these results, it can be established that As(V) and As(III) adsorption results fit better the Elovich model.

3.2.3 Ions interference effect on As(V) adsorption

To emulate real waters conditions, the interference of different ions and different water matrices was assessed. The obtained results for arsenate removal are presented in Figure 7.

As was observed by other authors [14, 16, 17], the addition of NO_3^-, SO_4^{-2} and Cl^- did not cause a significant reduction of As(V) adsorption, by using MA. The complexes formed with these anions may be much weaker (outer sphere complex) than those formed between arsenate and MA [15, 18].

In contrast with outer-sphere complexation, the adsorption through inner-sphere complexation is not greatly influenced by the alteration of the ionic strength of the solution [49]. However, from our results, the pH dependency of the adsorption process indicates a strong electrostatic attraction mechanism. Therefore, it is possible that the arsenic oxyanions are predominantly adsorbed non-specifically by strong electrostatic attraction, followed by a strong inner-sphere complexation between arsenic oxyanions and surface hydroxyl groups on the surface of the studied adsorbents [15, 49].

In the case of MA-5Fe, the effect of the interfering ions resulted stronger, which may indicate that the bond between arsenate and MA-5Fe could be weaker than the bond formed with MA. The effect of chloride has been ascribed to complexing between chloride and iron(III) as well as competition with arsenic species for adsorption sites [50].

When checking tap water, the As(V) adsorption increased for both materials. Studies reported that the addition of an electrolyte could increase the adsorption levels due to the depression of negative solid surface charges in the alkaline region [51]. Chen et al [11], studied the effect of different ions during arsenic adsorption onto ferric impregnated volcanic ash. The authors observed that all of the investigated coexisting cations (K^+, Ca^{2+}, and Fe^{3+}) enhanced As(V) removal. Zhang et al. [39] observed the same behavior in the case of Ca^{2+}, and reported that metallic cations can link the adsorbent particle with arsenate, forming a metal–arsenate complex or a metal–H_2O–arsenate complex. In our study, the increased arsenate removal in tap water may be related to the presence of co-existing cations such as Ca^{2+} and Na^+, as observed in the study of Chen et al [11], when using tap and lake water.

In contrast with the insignificant interference observed in the presence of NO_3^-, SO_4^{-2} and Cl^-, phosphate had a very detrimental effect on As(V) adsorption, as it was reported by other studies [14, 18, 26, 51]. Phosphate can compete with arsenate for binding sites on Fe_2O_3 and Al_2O_3 due to the similarity of their structure (charge, same tetrahedral configuration).

3.2.4 FTIR & XPS analysis of adsorption mechanism

According to several studies, the arsenic adsorption mechanism involves electrostatic attraction and surface complexation processes. It has been reported that As(V) forms predominantly inner-sphere bidentate binuclear complexes with Al/Fe oxides [8, 10, 14, 50-52]. For As(III), the co-existence of inner and outer sphere adsorption complexes was observed [8, 50].

Inner-sphere surface complexes are created as a result of direct chemical bond formation between the adsorbing anion (Lewis base) and the surface (Lewis acid) [8]. These complexes are formed via a ligand exchange reaction with a surface functional group, and as a result, no water molecules are present between surface functional groups and the adsorbate ions. On the other hand, outer-sphere surface complexes are formed as a result of electrostatic attraction between opposite charges [36]. The model of outer-

sphere complex formation presumes that ions can also be bound to the surface sites by chemical bonds without losing their hydration water. This means that a water molecule is located between the adsorbate ion and the adsorption site. Therefore, the distance to the surface is larger and the binding strength is weaker in comparison to inner-sphere complex formation [36].

In addition to sorption reactions, the formation of a small quantity of newly formed secondary oxides and their co-precipitation with the target metal(loid)s (e.g., $FeAsO_4.H_2O$, $FeAsO_4.2H_2O$, and $Fe_3(AsO_4)_2$) is another important removal mechanism [53].

In order to investigate the interaction between Al/Fe oxides and As, FTIR measurements were performed with samples before and after As(V) adsorption (initial concentration 100 mg/L) at the equilibrium pH values of 4, 8 and 10 (Figs. 8 and 9). Both materials showed common peaks at 3400, 1635, 500 cm^{-1}. The broad peak centered on 3400 cm^{-1} is attributed to the presence of hydrogen bonded hydroxyl groups which are also responsible for the absorption band at around 1635 cm^{-1} ((HOH)-bending mode for water). The broad peak centered around 500-550 cm^{-1} is assigned to the stretch vibration of Al–O(AlO_6) [26].

In some of the spectra, the intensity of the 3400 cm^{-1} broad peak decreased after As(V) adsorption, suggesting that hydroxyl groups are replaced to bond As(V) [13, 23]. This was observed in the case of MA, especially at lower pH, due to the stronger electrostatic interaction between $H_2AsO_4^-$ and the protonated hydroxyl groups. This also occurred in the case of MA-5Fe at pH 4. However, in sample MA-5Fe, at pH > PZC, the broad bands at 3400 and 500 cm^{-1} intensified. This may be related to species formed during iron/aluminum–arsenic co-precipitation caused by the formation of iron/aluminum (hydro)oxides [11]. Hu et al [54] studied the coagulation of As(V) using $FeCl_3$ and $AlCl_3$. FTIR measurements performed in this study indicated a shift of the peak assigned to the stretching vibration Al-O (606 cm^{-1}) to a lower value (559 cm^{-1}) after As(V) complexation. In the MA-5Fe samples at pH >PZC, attenuation of 670 cm^{-1} peak with intensification of 500-600 cm^{-1} peaks was observed, which may be related to the substitution of -OH with As-O during coagulation/precipitation.

A very small band appeared at 1030 cm^{-1} (Al-O-H vibration), which slightly shifted (1040-1050 cm^{-1}) after As(V) adsorption, especially at pH > PZC, which could be attributed to the interaction between Al-O-H group and arsenic species [26].

In the case of MA, the broad band at 550 cm^{-1} was reduced after As(V) adsorption, indicating a considerable reduction of metal oxygen bending vibration after the arsenic adsorption (arsenate may strongly interact with the surface oxide) [13].

Studies reported that the presence of arsenate is resolved by a band in the 856-866 cm^{-1} region [57]. However, it is difficult to distinguish the As-O bond peak due to overlap with Al-O peak (840-850 cm^{-1}) [23, 55].

XPS measurements were also performed with samples before and after As(V) adsorption (initial concentration 500 mg/L) at the equilibrium pH values of 4, 8 and 10 and after As(III) adsorption (initial concentration 100 mg/L) at the equilibrium pH 8.

XPS confirmed the presence of As in the adsorbent samples. New As 3d peaks at 44.5-44.8 eV for As(V) and 43.3-43.6 eV for As(III) were observed after adsorption (Table 9). No change in the arsenic oxidation state was observed after the tests.

In most experiments, the Al 2p and Fe 2p peaks shifted towards higher or lower binding energies after As adsorption tests (Table 10) [23, 54]. The binding energy change may be attributed to the interaction between arsenic and Al/Fe species present in the oxides due to ligand exchange reaction [56], and it is more noticeable at neutral to basic pH since variations lower than ±0.2 eV may account for experimental error. Differences in the XPS peaks shift are connected to different initial pH, arsenic speciation and surface complexes (inner-sphere: bidentate binuclear, bidentate mononuclear, monodentate binuclear and monodentate mononuclear; or outer-sphere complexes) [23]. Some authors reported that different kinds of surface complexes can cause either a positive or negative Al 2p peak shift in materials such as Fe/Al hydroxides, when adsorbing different arsenate speciation, indicating that this peak displacement might not be necessarily consistent even though an As-O-Al bond is formed.

For both adsorbents, the As/Al surface ratio decreased as pH increased, in concordance with their poorer adsorption performance at high equilibrium pH values, due to the electrostatic repulsion between arsenic species and the adsorbents surface (Table 9).

3.2.5. Desorption studies

Significant desorption levels were registered in the alkaline pH range. At pH_0 = 11.5, a desorption around 42 % was obtained with MA and MA-5Fe materials. The higher concentration of hydroxyl anions led to the ion exchange desorption of arsenate ions.

Nevertheless, a loss of Al_2O_3/Fe_2O_3 around 6 % was detected after the desorption experiment. At pH_0 = 12, almost complete arsenate desorption was achieved. However, around 16.5 % of Al_2O_3 was dissolved in both adsorbents, with 12 % loss of Fe_2O_3 in the MA-5Fe sample.

The arsenate desorption at high pH values may be also related to the dissolution of the materials in the alkaline region. During the desorption test, it was observed the formation of a heterogeneous emulsion, that could be easily eliminated through centrifugation or filtration. Therefore, at basic pH values, the arsenic removal through dissolution and co-precipitation with Al or Fe oxy-hydroxides cannot be discarded [6].

Negligible desorption was observed in the acidic/neutral pH range. Between pH_0 3.5-7.5, the adsorbents were stable and no metal leaching was detected.

Conclusions

Mesoporous alumina (MA) and mesoporous Fe doped alumina (MA-5Fe) were prepared by a facile sol-gel route at room temperature. The materials revealed an ordered pore structure with narrow channels of ca. 10nm and amorphous walls. The synthetized adsorbents demonstrated to be very effective for As(V) and As(III) removal, with maximum As(V) uptakes of 90 and 62 mg/g at an equilibrium pH of 4, for MA and MA-5Fe, respectively. While at nearly neutral pH, maximum As(V) uptakes of 48 and 41 mg/L and As(III) uptakes of 16 and 10 mg/L, were obtained with MA and MA-5Fe, respectively.

The synthetized materials displayed an important arsenic uptake capacity in comparison to a commercial alumina sample and in relation to similar metal oxides systems reported in the literature. This high adsorption capacity is connected to its amorphous nature and enhanced surface and structural properties: uniform accessible mesopores and surface acidity.

The Fe doped adsorbent showed a higher adsorption capacity per square meter of surface area (strong arsenate affinity). In this sense, it would be desirable to optimize the sol-gel synthesis conditions to increase its surface area and improve the adsorption capacity.

FTIR and XPS measurements evidenced the interaction between Al/Fe oxides and the arsenic species. The adsorption process may be based on the ligand exchange adsorption mechanism and the electrostatic interaction related to the solution pH, arsenic speciation and samples PZC.

Arsenate desorption was achieved under alkaline conditions. However, the stability of the materials may be compromised depending on the alkaline solution concentration.

In general, arsenic isotherms adjusted well to the Freundlich model and more accurately to the three parameters Sip´s model. The kinetics results fitted the Elovich model.

Under the studied operating conditions, the addition of interfering ions (NO_3^-, SO_4^{-2} and Cl^-) did not cause a significant reduction of As(V) adsorption using MA. However, phosphate had a very detrimental effect on As(V) adsorption due to its similar structure with arsenate. Additionally, the use of a tap water matrix increased arsenate adsorption in both materials, indicating a favorable perspective for the use of these materials in the treatment of real effluents.

4. Acknowledgements

This work was supported by CONICET (PIP-0575), UNMdP, ANPCyT (PICT1992-2014) (Argentina), the Spanish Ministry funding (CTM2015-65414-C2-1-R), Marie Skłodowska-Curie Actions: Research and Innovation Staff Exchange (RISE): "Advanced multifunctional materials applied to remove arsenic in Argentinian groundwater" (NANOREMOVAS).

5. Nomenclature

C_0: Aqueous concentration of arsenic at initial time (mg/L)

C_E: Aqueous concentration of arsenic at equilibrium (mg/L)

d_{pore}: Average pore diameter (nm)

k_1: Pseudo-first order rate constant (min^{-1})

k_2: Pseudo-second order rate constant ($g\ mg^{-1}\ min^{-1}$)

α: Elovich initial adsorption rate ($g\ mg^{-1}\ min^{-2}$)

β: Elovich desorption coefficient ($mg\ g^{-1}\ min^{-1}$)

k_p: Intra-particle diffusion model rate constant ($mg\ g^{-1} min^{-1}$)

C: Intra-particle diffusion model constant, related to thickness of boundary layer ($mol^2\ J^{-2}$).

K_{RD}: DR constant related to sorption energy ($mol^2\ J^{-2}$)

A: Temkin equilibrium constant ($l\ mg^{-1}$)

B: Temkin variation of adsorption energy (J/mol)

K_a: Sip's adsorption affinity constant, where i stands for the pH_{eq} value (L/mg)

K_F: Freundlich adsorption coefficient per gram of adsorbent ($mg^{n-1} \cdot L^n/g$)

K'_F: Freundlich adsorption coefficient per square meter of adsorbent ($mg^{n-1} \cdot L^n/m^2$)

K_L: Langmuir adsorbent-adsorbate affinity constant (L/mg)

n: Freundlich isotherm exponent

u: Sip's model exponent

pH_0: Initial pH value

pH_{eq}: Equilibrium pH value

PZC: pH value of point of zero charge

qe: Solid phase concentration of arsenic at equilibrium (mg/g)

qt: Solid phase concentration of arsenic at any time (mg/g)

Q_a: Maximum adsorption capacity per gram of adsorbent, Sip´s model (mg/g)

Q'_a: Maximum adsorption capacity per square meter of adsorbent, Sip´s model (mg/m^2)

Q_Em: Maximum adsorption capacity per gram of adsorbent (mg/g)

Q'_Em: Maximum adsorption capacity per square meter of adsorbent (mg/m^2)

Q_E: Adsorption capacity per gram of adsorbent (mg/g)

Q'_E: Adsorption capacity per square meter of adsorbent (mg/m^2)

Qm: Maximum saturated monolayer adsorption capacity per gram of adsorbent (mg/g)

Q'm: Maximum saturated monolayer adsorption capacity per square meter of adsorbent (mg/m^2)

Q_{RD}: Maximum adsorption capacity DR model (mg/g)

RT: Room temperature

S_{BET}: Specific surface area (m^2/g)

V: Volume of the arsenic solution (L)

V_{pore}: Pore volume (cm^3/g)

REFERENCES

1. Arsenic in Drinking-water Background document for development of WHO Guidelines for Drinking-water Quality © World Health Organization 2011.
2. M. Jang, S-H. Ming, J. K. Park, E. J. Tlachac, Hydrous ferric oxide incorporated diatomite for remediation of arsenic contaminated groundwater, Environ. Sci. Technol. 41 (2007) 3322-3328.
3. Y-F. Pan, C. T. Chiou, T-F. Lin, Adsorption of arsenic(V) by iron-oxide-coated diatomite (IOCD), Environ Sci. Pollut. Res. 17 (2010)1401–1410.

4. M. I. Litter, M. E. Morgada, J. Bundschuh, Review: Possible treatments for arsenic removal in Latin American waters for human consumption, Environ.Pollut. 158 (2010) 1105–1118.
5. H. Malik, Z. M. Khan, Q. Mahmood, S. Nasreen, Z. A. Bhatti, Review: Perspectives of low cost arsenic remediation of drinking water in Pakistan and other countries, J. Hazard. Mat. 168 (2009) 1–12.
6. K. Henke, Arsenic: Environmental Chemistry, Health Threats and Waste Treatment, Wiley, Chippenham 2009.
7. D. Mohan, C. U. Pittman Jr., Arsenic removal from water/wastewater using adsorbents—A critical review, J. Hazard. Mat. 142 (2007) 1–53.
8. B. Kasprzyk-Hordern, Chemistry of alumina, reactions in aqueous solution and its application in water treatment, Adv. Colloid Interface Sci. 110 (2004) 19–48.
9. S. Luther, N. Borgfeld, J. Kim, J.G. Parsons, Removal of arsenic from aqueous solution: A study of the effects of pH and interfering ions using iron oxide nanomaterials, Microchem. J. 101 (2012) 30–36.
10. M. Dai, L. Xia, S. Song, C. Peng, A. Lopez-Valdivieso, Adsorption of As(V) inside the pores of porous hematite in water, J. Hazard. Mat. 307 (2016) 312–317.
11. R. Chen, Z. Zhang, Y. Yang, Z. Lei, N. Chen, X. Guo, C. Zhao, N. Sugiura, Use of ferric-impregnated volcanic ash for arsenate (V) adsorption from contaminated water with various mineralization degrees, J. Colloid Interface Sci. 353 (2011) 542‑548.
12. Y. Mamindy-Pajany, C. Hurel, N. Marmier, M. Roméo, Arsenic (V) adsorption from aqueous solution onto goethite, hematite, magnetite and zero-valent iron: Effects of pH, concentration and reversibility, Desalination 281 (2011) 93–99.
13. T. Basu, K. Gupta, U. C. Ghosh, Performances of As(V) adsorption of calcined (250◦C) synthetic iron(III)–aluminum(III) mixed oxide in the presence of some groundwater occurring ions, Chem. Eng. J. 183 (2012) 303– 314.
14. V. K. Tchieda, E. D'Amato, A. Chiavola, M. Parisi, A. Chianese, M. Amamra, A. Kanaev, Removal of arsenic by alumina: Effects of material size, additives, and water contaminants, Clean – Soil, Air, Water 44 (5) (2016) 496–505.

15. T. Mahmood, S.U. Din, A. Naeem, S. Mustafa, M. Waseem, M. Hamayun, Kinetics, equilibrium and thermodynamics studies of arsenate adsorption from aqueous solutions onto iron hydroxide, Chem. Eng. J. 192 (2012) 90-98.

16. M. A. Anderson, J. F. Ferguson, J. Gavis, Arsenate adsorption on amorphous aluminum hydroxide, J. Colloid Interface Sci. 54:3 (1976) 391-399.

17. L. Zheng, Arsenic adsorption from aqueous solutions on an Fe(III)-Si binary oxide adsorbent, Water Qual. Res. J. Canada, 39:3 (2004) 267–275.

18. Y. Jeong, F. Maohong, J. Van Leeuwen, J. F. Belczyk, Effect of competing solutes on arsenic(V) adsorption using iron and aluminum oxides, J. Environ. Sci. 19 (2007) 910–919.

19. S. Kuriakose, T. S. Singh and K. K. Pant, Adsorption of As(III) from aqueous solution onto iron oxide impregnated activated alumina, Water Qual. Res. J. Canada 39: 3 (2004) 258–266.

20. S. S. Tripathy, A. M. Raichur, Enhanced adsorption capacity of activated alumina by impregnation with alum for removal of As(V) from water, Chem. Eng. J. 138 (2008) 179–186.

21. T. S. Singh, K.K. Pant, Equilibrium, kinetics and thermodynamic studies for adsorption of As(III) on activated alumina, Sep. Purif. Technol. 36 (2004) 139–147.

22. M-J. Yu, X. Li, W-S. Ahn, Adsorptive removal of arsenate and orthophosphate anions by mesoporous alumina, Microporous Mesoporous Mater. 113 (2008) 197‑203.

23. W. Li, D. Chen, F. Xia, J. Z. Y. Tan, P-P. Huang, W-G. Song, N. M. Nursam, R. A. Caruso, Extremely high arsenic removal capacity for mesoporous aluminium magnesium oxide composites, Environ. Sci.: Nano 3 (2016) 94.

24. Maiti, J. Kumarbasu, S. De, Fe-Al nano-oxide prepared by sol-gel method using precursor of HCl digested liquid fraction of laterite: Arsenic adsorption performance, Int. J. Nanosci. 10:4, 5 (2011) 1173-1177.

25. N. Chubar, New inorganic (an)ion exchangers based on Mg‑Al hydrous oxides: (Alkoxide-free) sol‑gel synthesis and characterisation, J. Colloid Interface Sci. 357 (2011) 198‑209.

26. C. Han, H. Pu, H. Li, L. Deng, S. Huang, S. He, Y. Luo, The optimization of As(V) removal over mesoporous alumina by using response surface

methodology and adsorption mechanism, J. Hazard. Mat. 254– 255 (2013) 301–309.

27. C. Márquez-Alvarez, N. Žilková, J. Pérez-Pariente, J. Čejka, Synthesis, characterization and catalytic applications of organized mesoporous aluminas, J. Catal. Rev. 50 (2008) 222–286.
28. M. Trueba, S.P. Trasatti, γ-Alumina as a support for catalysts: A review of fundamental aspects, Eur. J. Inorg. Chem. 17 (2005) 3393–3403.
29. S. David, J. & Justin S. J., H. Metal Oxide Catalysis. WILEY-VCH Verlag GmbH & Co. KGaA, 2009.
30. Q. Yuan, A. Yin, C. Luo, L. Sun, Y. Zhang, W. Duan, H. Liu and C. Yan, Facile synthesis for ordered mesoporous γ-aluminas with high thermal stability, J. Am. Chem. Soc. 130 (2008) 3465–34729.
31. W. Cai, J. Yu, C. Anand, A. Vinu and M. Jaroniec, Facile synthesis of ordered mesoporous alumina and alumina-supported metal oxides with tailored adsorption and framework properties, Chem. Mater. 23 (2011) 1147–1157.
32. F. Fu, Z. Cheng, J. Lu, Synthesis and use of bimetals and bimetal oxides in contaminants removal from water: a review, RSC Adv., 5 (2015) 85395-85409.
33. R.K. Dhar, Y. Zheng, J. Rubenstone, A. van Geen, A rapid colorimetric method for measuring arsenic concentrations in groundwater, Anal. Chim. Acta 526 (2004) 203–209.
34. Langmuir, The adsorption of gases on plane surfaces of glass, mica and platinum, J. Am. Chem. Soc., 40 (1918) 1361-1403.
35. K.Y. Foo, B.H. Hameed, Review: Insights into the modeling of adsorption isotherm systems, Chem. Eng. J. 156 (2010) 2–10.
36. Worch, Adsorption Technology in Water Treatment Fundamentals, Processes, and Modeling, 1st ed., de Gruyter, Göttingen 2012.
37. J. Febrianto, A. N. Kosasih, J. Sunarso, Y-H Ju, N. Indraswati, S. Ismadji, Review: Equilibrium and kinetic studies in adsorption of heavy metals using biosorbent: A summary of recent studies, J. Hazard. Mat. 162: 2–3 (2009) 616-645.
38. G. P. Jeppu, T. P. Clement, A modified Langmuir-Freundlich isotherm model for simulating pH-dependent adsorption effects, J. Contam. Hydrol. 129–130 (2012) 46–53.

39. J. Zhang, R. Stanforth, Slow adsorption reaction between arsenic species and goethite (r-FeOOH): Diffusion or heterogeneous surface reaction control, Langmuir 21 (2005) 2895-2901.
40. W.J. Weber Jr., J.C. Morris, J. Sanit, Kinetics of adsorption on carbon from solution, Journal of the Sanitary Engineering Division, American Society of Civil Engineers, 89 (1963) 31-38.
41. M. Thommes, K. Kaneko, A.V. Neimark, J.P. Olivier, F. Rodriguez-Reinoso, J. Rouquerol, K.S.W. Sing, Physisorption of gases, with special reference to the evaluation of surface area and pore size distribution, IUPAC Technical Report Pure and Applied Chemistry 87 (9-10) (2015) 1051–1059.
42. M. Kosmulski, pH-dependent surface charging and points of zero charge III. Update, J. Colloid Interface Sci. 253 (2002) 77–87.
43. L. M. Camacho, S. Ponnusamy, I. Campos, T. A. Davis, S. Deng in: SIS Flora (Ed), Handbook of arsenic toxicology: Evaluation of novel modified activated alumina as adsorbent for arsenic removal, Elsevier, 2015, pp. 121-136.
44. García-Sanchez, E. Alvarez-Ayuso, F. Rodriguez-Martin, Sorption of As(V) by some oxyhydroxides and clay minerals. Application to its immobilization in two polluted mining Soils, Clay Miner. 37 (2002) 187–194.
45. X. Carrier, E. Marceau, J. F. Lambert, M. Che, Transformations of γ -alumina in aqueous suspensions 1. Alumina chemical weathering studied as a function of pH, J. Colloid Interface Sci. 308 (2007) 429–437.
46. G. Lefevre, M. Duc, P. Lepeut, R. Caplain and M Fedoroff, Hydration of γ -alumina in water and its effects on surface reactivity, Langmuir 18 (2002) 7530-7537.
47. M. B. McBride and L. G. Wessellnkt, Chemisorption of catechol on gibbsite, boehmite, and noncrystalline alumina surfaces, Environ. Sci. Technol. 22 (1998) 703-708.
48. L. Mercier and T. J. Pinnavaia, Access in mesoporous materials: Advantages of a uniform pore structure in the design of a heavy metal ion adsorbent for environmental remediation, Adv. Mater. 9:6 (1997) 500-503.
49. J. Hua, Adsorption of low-concentration arsenic from water by co-modified bentonite with manganese oxides and poly(dimethyldiallylammonium chloride), J. Environ. Chem Eng. 6:1 (2018) 156-168.

50. D. E. Giles, M. Mohapatra, T. B. Issa, S. Anand, P. Singh, Review: Iron and aluminium based adsorption strategies for removing arsenic from water, J. Environ. Manage. 92 (2011) 3011-3022.
51. W. Zhang, P. Singh, E. Paling, S. Delides, Arsenic removal from contaminated water by natural iron ores, Miner. Eng. 17 (2004) 517–524.
52. K. Mandal, K. T. Suzuki, Arsenic round the world: a review, Talanta 58 (2002) 201–235.
53. M. Komárek, A. Vanëk, V. Ettler, Review: Chemical stabilization of metals and arsenic in contaminated soils using oxides e A review, Environ. Pollut. 172 (2013) 9-22.
54. C. Hu, Q. Chen, H. Liu, J. Qu, Coagulation of methylated arsenic from drinking water: Influence of methyl substitution, J. Hazard. Mat. 293 (2015) 97–104.
55. S. Goldberg, and C. T. Johnston, Mechanisms of arsenic adsorption on amorphous oxides evaluated using macroscopic measurements, vibrational spectroscopy, and surface complexation modeling, J. Colloid Interface Sci. 234 (2001) 204–216.
56. H. Li, L. Zhang, H. Dai, H. He, Facile synthesis and unique physicochemical properties of three-dimensionally ordered macroporous magnesium oxide, gamma-alumina, and ceria-zirconia solid solutions with crystalline mesoporous walls, Inorg. Chem. 48 (2009) 4421-4434.
57. L. Sigg L, W. Stumm, Aquatische Chemie [Aquatic Chemistry]. Zurich: vdf Hochschulverlag; 2011.

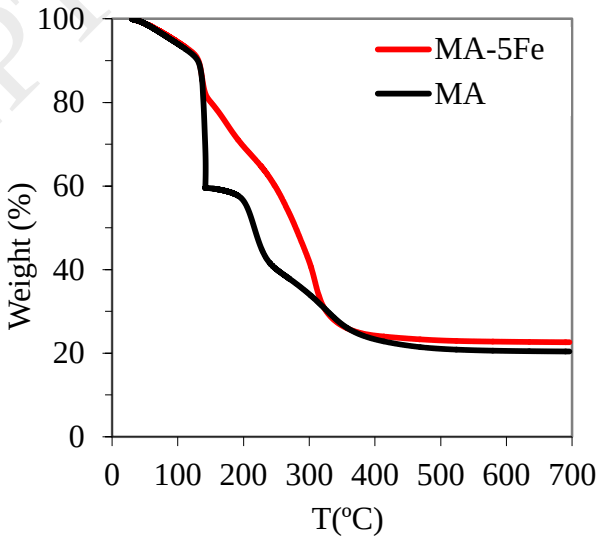

Fig 1. Thermogravimetric analysis of MA and MA-5Fe xerogels before calcination step.

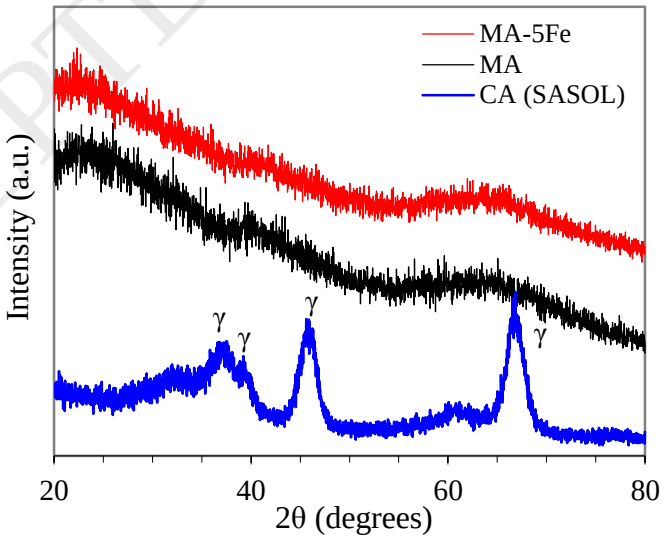

Fig 2. XRD diffractograms of the tested adsorbents.

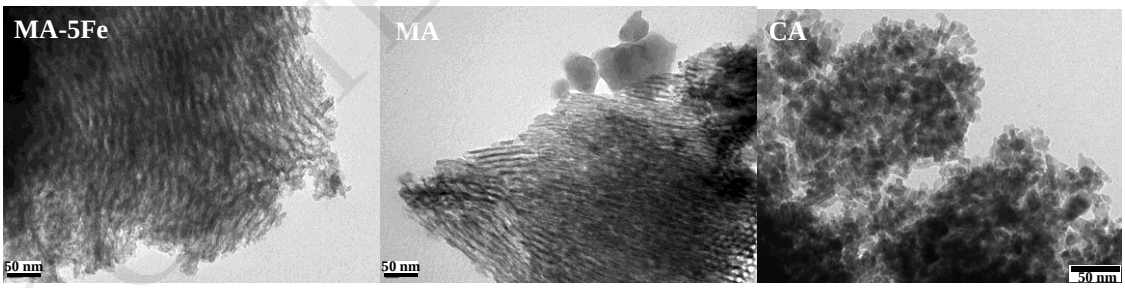

Fig 3. TEM images of the different tested alumina adsorbents.

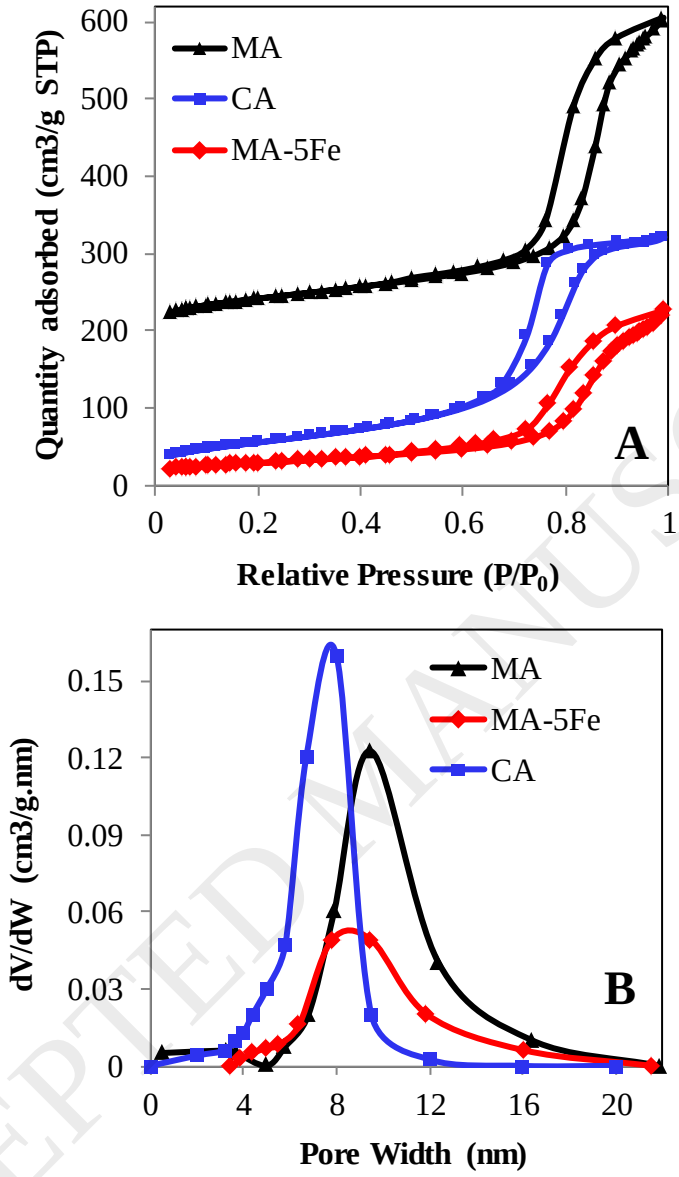

Fig 4. N_2 Physisorption results: isotherms at -196 °C (A) and pore size distribution (B).

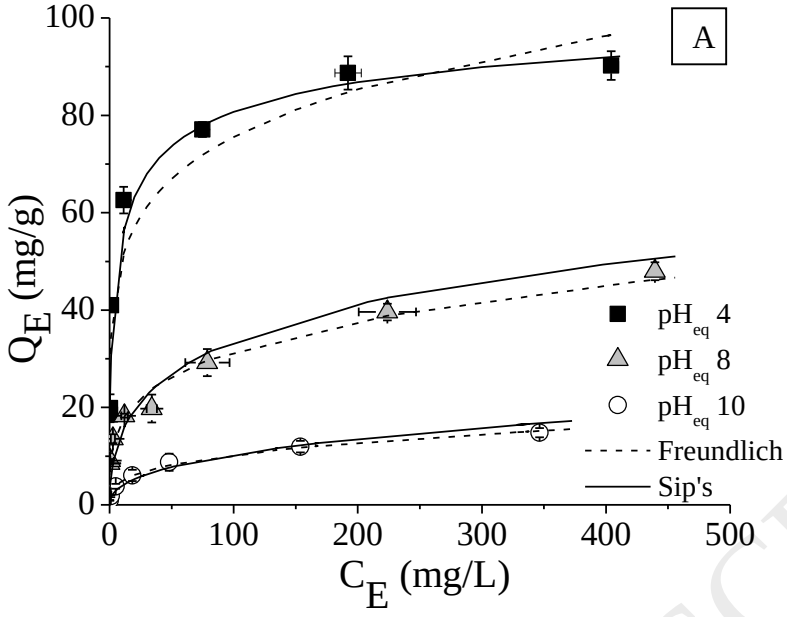

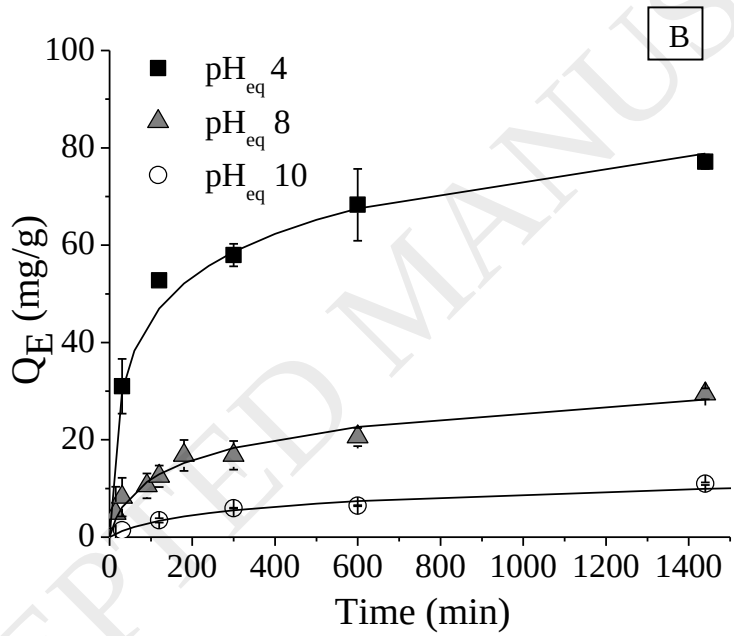

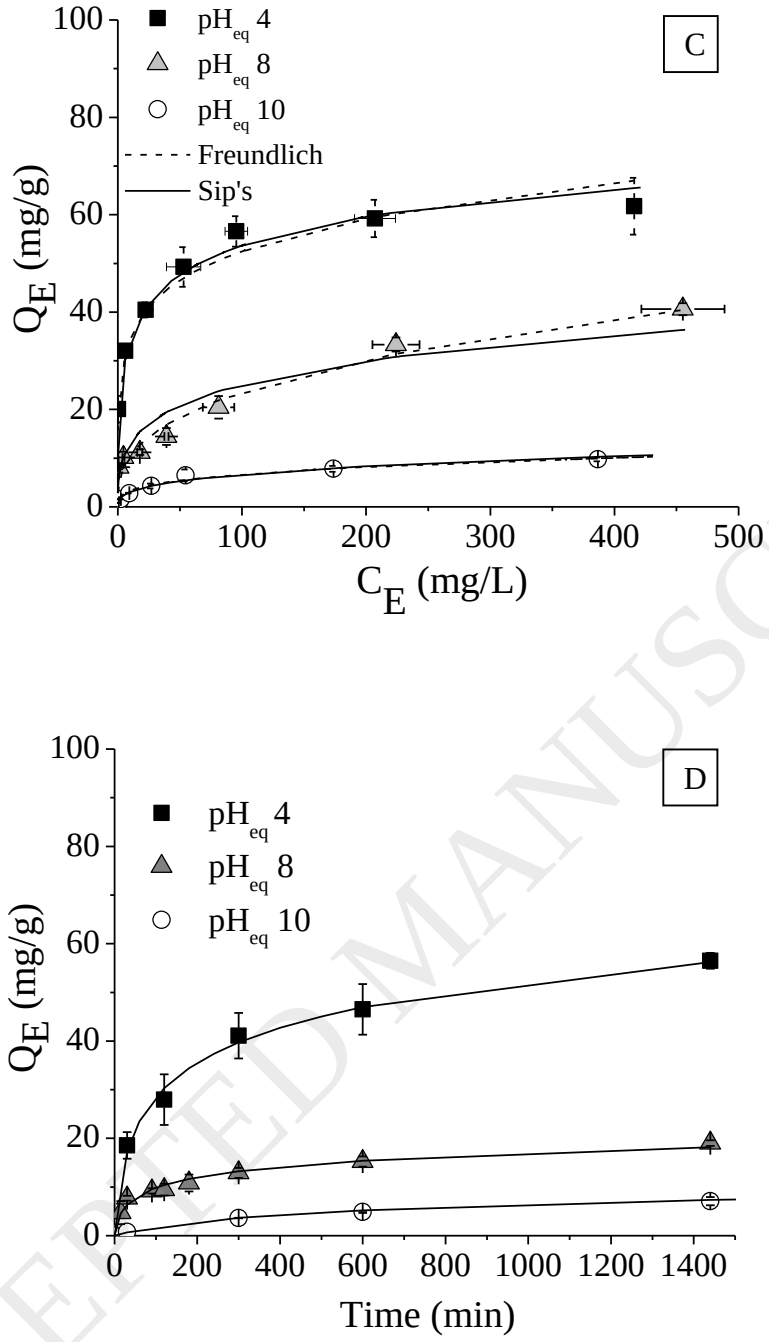

Fig 5. As(V) adsorption at different pH equilibrium values (25ºC): A) MA isotherms, B) MA kinetic curves (C_0 = 100 mg/L), C) MA-5Fe isotherms and D) MA-5Fe kinetic curves (C_0 = 100 mg/L). Isotherms curves: solid line-Sips model and dash line-Freundlich model. The kinetic curves correspond to the Elovich model.

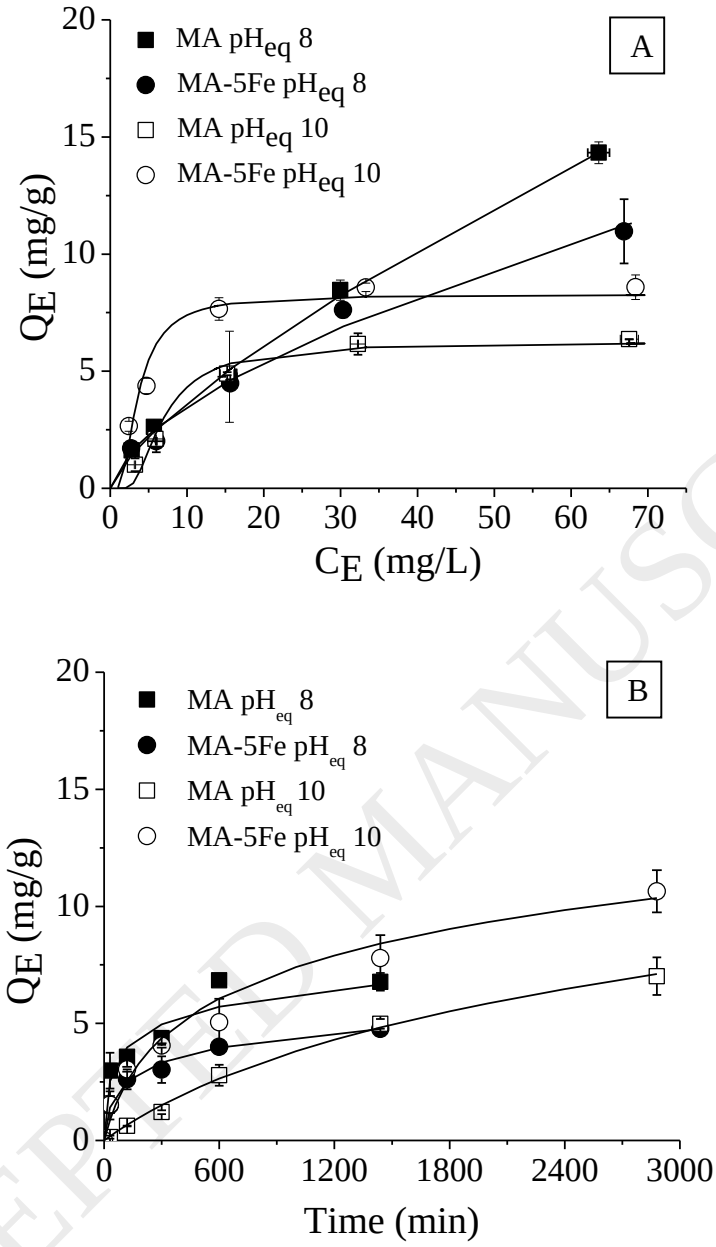

Fig 6. As(III) adsorption at different pH equilibrium values (25ºC): A) MA and MA-5Fe isotherms and B) MA and MA-5Fe kinetic curves (C_0 = 20 mg/L). Isotherms curves correspond to the Freundlich model at pH 8 and the DR model at pH 10. Kinetic curves at pH 8 correspond to the Elovich model.

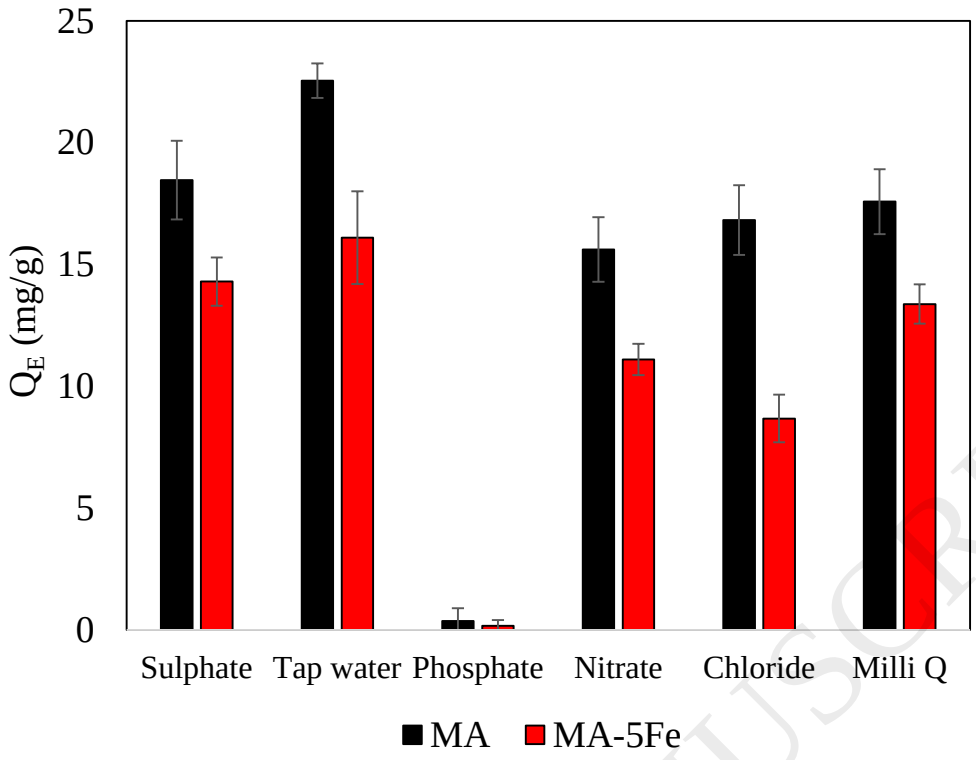

Fig 7. Anions interference effect on As(V) adsorption capacity for MA and MA-5Fe ([As(V)]:[anion]$_{mol}$ = 1:25, pH_{eq} = 8, T = 25ºC).

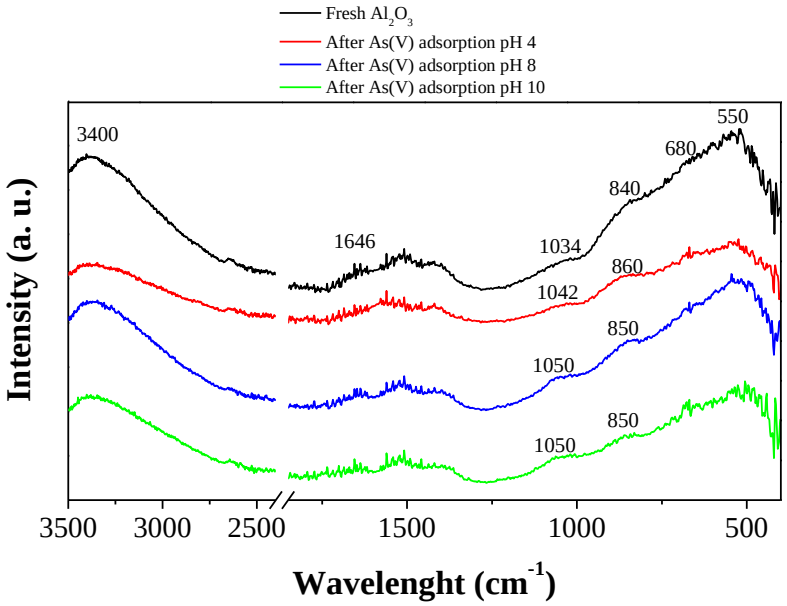

Fig. 8. FTIR of fresh and used samples of MA in the adsorption of As(V) under different pH values (4, 8, 10).

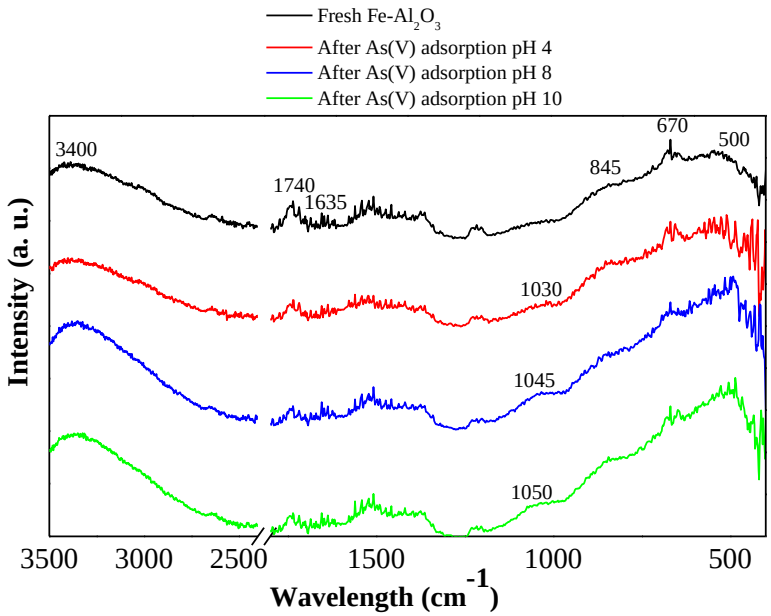

Fig. 9. FTIR of fresh and used samples of MA-5Fe in the adsorption of As(V) under different pH values (4, 8, 10).

Table 1. Results presented by other authors employing alumina or iron oxides for arsenic removal.

Adsorbent	pH_{eq}	Surface area (m^2/g)	T (ºC)	Capacity (mg/g)		Reference
				As(V)	As(III)	
IOCD-20,11 (diatomite/Fe)	5.5	93.0	30	8.60	-	3
Fe_2O_3	6	-	RT	4.60	1.25	9
Fe_3O_4	6	-	RT	6.70	8.20	9
Hematite	7	4.36	25	0.900	-	10
Goethite	7	58.2	25	7.60	-	10
Siderite	7	39.7	25	8.10	-	10
Ferric impregnated volcanic ash	7	147	20	5.30	-	11
Hematite	6	1.66	25	3.30	-	12
Goethite	6	11.6	25	1.40	-	12
Zero valent iron	6	0.200	25	30.1	-	12
Magnetite	6	1.60	25	7.10	-	12
Synthetic Fe-Al mixed oxides	7	131	30	54.5	-	13
Mesoporous γ-Al_2O_3	6.5-7	110	RT	19.8	-	14
Mixed oxide Fe/Si	5-8	198	25	20.7-12.9	-	15
Amorphous aluminum hydroxide	7	-	RT	164	-	16
Fe/Si oxide	6.5	186	20.5	11.3	21.4	17
Fe_2O_3	6	5.05	25	0.616	-	18
Al_2O_3	6	0.550	25	0.098	-	18
Iron oxide impregnated activated alumina	12	200	25	-	0.734	19
Alum impregnated activated alumina	7	183		5.57	-	20
Activated alumina	7.6	370	25	-	0.180	21
Mesoporous alumina	8	483	RT	61.3	-	22

Commercial activated alumina	8	322	RT	12.1	-	22
Meso-Al-400	7	396	RT	299	110	23
Meso-80Al20Mg-400	7	422	RT	225	391	23
Nanoparticle Fe-Al oxide		68.9	32	20.7	6.20	24
Mg-Al hydrous oxide	7	290	22	220	-	25
Mesoporous alumina	4	312	52.8	39.1	-	26
Mesoporous alumina	6.6	312	25	36.6	-	26
Al_2O_3 (MA)	4	221	25	90.0	-	*This study*
Fe-Al_2O_3 (MA-5Fe)	4	104	25	62.0	-	*This study*
γ-Al_2O_3 (CA)	4	200	25	54.0	-	*This study*
Al_2O_3 (MA)	8	221	25	48.0	16.0	*This study*
Fe-Al_2O_3 (MA-5Fe)	8	104	25	41.0	10.0	*This study*
γ-Al_2O_3 (CA)	8	200	25	36.0	-	*This study*

Table 2. Summary of N_2-physisorption outcomes.

Sample	PZC	S_{BET} (m^2/g)	V_{pore} (cm^3/g)	d_{pore} (nm)
MA	7.5	221	0.66	10.2
MA-5Fe	7.5	104	0.34	9.67
CA	7.5	200	0.50	7.15

Table 3. TPD of pyridine results.

Sample	**Quantity of acid sites** (mmol/g)	**Density of acid sites** (mmol/m^2)	**Pyridine desorption temperature** (^oC)
MA	0.130	0.0006	235
MA-5Fe	0.200	0.0020	235
CA	0.097	0.0005	227

Table 4. As(V) and As(III) maximum adsorption capacities for all materials tested. As(V): 0.5 g/L of adsorbent at pH_0 3.7 and 7.5, and 5 g/L at pH_0 11.5. As(III): 0.5 g/L of adsorbent at all initial pH of study. Time of experiment, 24 h; temperature, 25ºC.

		Maximum capacity Q_Em (mg/g)					**Maximum capacity Q'_Em** (mg/m^2)				
Initial pH	**pH_{eq}**	**MA**		**MA-5Fe**		**CA**	**MA**		**MA-5Fe**		**CA**
		As(V)	**As(III)**	**As(V)**	**As(III)**	**As(V)**	**As(V)**	**As(III)**	**As(V)**	**As(III)**	**As(V)**
3.7	**4**	90	-	62	-	54	0.41	-	0.60	-	0.27
7.5	**8**	48	16	41	10	36	0.22	0.07	0.39	0.10	0.18
11.5	**10**	15	7.2	10	7.6	-	0.07	0.03	0.10	0.07	-

Table 5. As(V) isotherms parameters (Langmuir. Freundlich. Temkin and DR)

Model	Parameters	pH_{eq} 4			pH_{eq} 8			pH_{eq} 10	
		MA	**MA-5Fe**	**CA**	**MA**	**MA-5Fe**	**CA**	**MA**	**MA-5Fe**
Langmuir	Qm (mg/g)	86.07	59.25	50.23	46.15	46.1	40.95	14.53	9.73
	Q'm (mg/m^2)	0.39	0.57	0.25	0.21	0.44	0.2	0.066	0.094
	K_L (L/mg)	0.59	0.16	0.13	0.031	0.012	0.0092	0.04	0.037
	R^2	0.95	0.82	0.67	0.73	0.84	0.83	0.92	0.91
	ERRSQ	690.62	1030.07	349.98	834.46	466.082	287.31	46.25	16.66
	HYBRID	79.56	346.53	120.18	378.81	228.64	188.03	41.2	20.76
	ARE	10.49	26.86	15.22	41.01	31.42	35.63	30.13	21.28
Freundlich	K_F ($mg^{n-1}.L^n/g$)	33.76	23.8	19.46	9.58	4.57	2.66	2.37	1.69
	K_F ($mg^{n-1}.L^n/m^2$)	0.15	0.23	0.097	0.043	0.044	0.013	0.011	0.016
	n	0.18	0.17	0.18	0.26	0.36	0.42	0.32	0.29
	R^2	**0.93**	**0.94**	**0.94**	**0.95**	**0.94**	**0.94**	**0.95**	**0.92**
	ERRSQ	988.81	350.62	65.88	148.87	106.11	97.53	30.11	16.03
	HYBRID	190.49	122.36	20.72	57.78	67.19	51.67	23.32	21.53
	ARE	18.3	15.98	5.97	13.72	16.73	18.08	22.26	20.82
Temkin	A (L/mg)	22.23	61.039	7.55	27.11	75	100	2.63	1.31
	B (J/mol)	237.7	399.1	362.96	614.63	900	1000	1258.74	1659.66
	R^2	**0.98**	**0.95**	**0.91**	0.77	0.59	0.27	0.91	0.92
	ERRSQ	315.11	285.84	99.52	1801.09	1157.37	1217.92	49.82	15.79
	HYBRID	46.75	65.78	33.63	646.43	249.88	685.42	58.39	24.28
	ARE	8.11	12.67	7.82	53.09	33.72	72.19	34.45	23.25
DR	Qm_{DR} (mg/g)	87.2	54.63	44.94	40.88	35.46	29.26	12.39	8.56
	$Q'm_{DR}$ (mg/m^2)	0.39	0.53	0.22	0.18	0.34	0.15	0.056	0.082
	K_{DR} ($(mol/J)^2$)	0.0000078	0.0000042	0.0000032	0.00016	0.00033	0.0004	0.000047	0.000085
	R^2	0.75	0.73	0.39	0.42	0.58	0.55	0.79	0.79
	ERRSQ	3479.703	1526.06	638.88	1801.091	1217.4	755.92	116.97	41.25
	HYBRID	811.5	460.7	198.31	696.43	505.67	440.38	115.28	70.32
	ARE	33.21	31.8	17.82	53.09	50.14	57.1	46.85	37.7

Table 6. As(V) Sip´s isotherm parameters

	MA	**MA-5Fe**	**CA**
Q_a (mg/g)	111.7	98.7	71.2
Q'_a (mg/m^2)	0.51	0.95	0.36
K_{a4} (L/mg)	0.1	0.0164	0.03549
K_{a8} (L/mg)	0.0013	0.00047	0.0011
K_{a10} (L/mg)	0.00004	0.0000058	-
n	0.41	0.35	0.046
R^2	**0.99**	**0.95**	**0.96**
ERRSQ	829.51	1653.23	312.07
HYBRID	69.61	81.52	61.86
ARE	16.23	18.015	16.78

Table 7. As(III) isotherms parameters (Langmuir. Freundlich. Temkin and DR).

Model	Parameters	pH_{eq} 8		pH_{eq} 10	
		MA	MA-5Fe	MA	MA-5Fe
Langmuir	Qm (mg/g)	15	12	6.4	9.87
	Q'm (mg/m^2)	0.068	0.12	0.029	0.095
	K_L (L/mg)	0.045	0.05	0.11	0.18
	R^2	0.84	0.91	0.88	0.95
	ERRSQ	34.93	11.85	9.28	5.15
	HYBRID	66.38	23.13	33.79	5.25
	ARE	22.25	18.82	35.02	7.72
Freundlich	K_F ($mg^{n-1}.L^n/g$)	0.67	0.86	1.06	3.04
	K_F ($mg^{n-1}.L^n/m^2$)	0.003	0.0083	0.0048	0.029
	n	0.74	0.61	0.45	0.27
	R^2	**0.96**	**0.96**	0.86	0.8
	ERRSQ	8.28	4.53	10.78	22.53
	HYBRID	25.46	10.44	37.62	26.54
	ARE	14.34	11.33	36.41	19.58
Temkin	A (L/mg)	0.36	0.42	0.57	2.15
	B (J/mol)	632.58	824.66	1292.32	1264.76
	R^2	0.84	0.89	0.94	0.89
	ERRSQ	34.82	12.85	4.24	12.5
	HYBRID	111.12	44.32	10.45	11.65
	ARE	39.48	30.14	18.27	12.03
DR	Qm_{DR} (mg/g)	14.33	10.93	6.23	8.27
	$Q'm_{DR}$ (mg/m^2)	0.065	0.11	0.028	0.08
	K_{DR} ((mol/J)^2)	0.000053	0.00004	0.0000067	0.0000021
	R^2	0.84	0.85	**0.95**	**0.92**
	ERRSQ	36.19	18.45	3.55	8.49
	HYBRID	124.03	86.65	18.63	12.22
	ARE	51.08	41.59	24.85	13.26

Table 8. As(V) kinetics parameters

Model	Parameters	pH_{eq} 4			pH_{eq} 8			pH_{eq} 10	
		MA	**MA-5Fe**	**CA**	**MA**	**MA-5Fe**	**CA**	**MA**	**MA-5Fe**
Pseudo First Order	k_1 (min^{-1})	0.0097	0.007	0.028	0.0042	0.0087	0.028	0.0019	0.0016
	R^2	0.88	0.89	0.96	0.82	0.72	0.78	0.94	0.98
	ERRSQ	945.66	360.12	53.27	377.95	181.82	64.48	10.39	1.41
	HYBRID	222.06	148.68	36.47	63.44	38.65	37.74	22.09	5.36
	ARE	13.92	16.19	7.54	12.56	10.44	11.39	17.51	10.18
Pseudo Second Order	k_2 ($g.mg^{-1}.min^{-1}$)	0.00023	0.00017	0.0012	0.00017	0.00073	0.0024	0.00016	0.00015
	R^2	0.97	0.94	0.98	0.87	0.84	0.83	0.97	0.98
	ERRSQ	251.32	199.68	16.28	270.4	106.79	47.63	5.95	1.59
	HYBRID	54.58	81.49	11.19	50.39	22.17	23.33	11.21	4.24
	ARE	6.56	12.21	3.97	12.59	7.07	9.1	11.77	8.15
Elovich	α ($g.mg^{-1}.min^{-1}$)	3.94	1.43	85.44	0.34	0.68	5.29	0.051	0.025
	β (mg/g)	0.077	0.094	0.24	0.15	0.32	0.52	0.32	0.36
	R^2	**0.98**	**0.97**	**0.98**	**0.91**	**0.93**	**0.87**	**0.98**	**0.97**
	ERRSQ	137.38	105.23	22.77	185.24	43.25	37.16	3.42	2.14
	HYBRID	29.96	37.18	12.38	61.62	10.44	13.89	4.97	3.75
	ARE	5.61	7.68	3.88	18.17	5.67	7.86	7.24	6.07
Intraparticle Diffusion	C_i (mg/g)	16.3	11.49	16.89	4.31	4.73	6.48	1.082	0.37
	K_i ($mg.g^{-1}.min^{-0.5}$)	1.89	1.32	0.82	0.68	0.41	0.29	0.22	0.18
	R^2	0.83	0.88	0.57	0.91	0.89	0.66	0.95	0.94
	ERRSQ	1373.03	383.86	506.88	189.38	73.73	97.95	8.33	4.91
	HYBRID	158.64	66	126.19	167.82	14.42	13.25	5.11	11.49
	ARE	11.81	10.13	14.28	30.11	6.06	6.14	5.36	12.44

Table 9. As(III) kinetics parameters.

Model	Parameters	pH_{eq} 8		pH_{eq} 10	
		MA	**MA-5Fe**	**MA**	**MA-5Fe**
Pseudo First Order	k_1 (min^{-1})	0.008	0.0066	0.0009	0.0015
	R^2	0.75	0.84	0.98	0.94
	ERRSQ	11.17	3.83	1.93	9.51
	HYBRID	32.42	17	5.74	30.79
	ARE	19.66	17.61	17.58	22.46
Pseudo Second Order	k_2 ($g.mg^{-1}.min^{-1}$)	0.002	0.0019	0.0002	0.00014
	R^2	0.84	0.91	0.91	0.95
	ERRSQ	6.94	2.23	7.2	8.11
	HYBRID	18.53	9.86	25.79	23.7
	ARE	15.91	12.16	43.26	19.12
Elovich	α ($g.mg^{-1}.min^{-1}$)	0.34	0.11	0.006	0.034
	β (mg/g)	0.91	1.1	0.22	0.34
	R^2	**0.92**	**0.95**	**0.99**	**0.96**
	ERRSQ	3.56	1.21	1.19	6.62
	HYBRID	8.59	5.97	3.86	15.12
	ARE	9.97	11.34	15.36	14.86
Intraparticle Diffusion	C_i (mg/g)	1.7	0.91	0	0.62
	K_i ($mg.g^{-1}.min^{-0.5}$)	0.15	0.11	0.12	0.19
	R^2	0.84	0.89	0.94	0.95
	ERRSQ	7.15	2.67	4.89	7.49
	HYBRID	8.77	7.93	73.61	10.74
	ARE	8.68	13.71	98.42	12

Table 10. XPS results (binding energy (eV) and atomic ratio) for MA and MA-5Fe samples fresh and used in As(V) and As(III) adsorption tests.

	Atomic ratio					Binding Energy (eV)				
	As(V)	**As(III)**	**Al**	**Fe**	**O**	**As(V)**	**As(III)**	**Al**	**Fe**	**O**
MA	-	-	31.4	-	68.6	-	-	73.4	-	530.0, 531.6
MA pH_{eq} 4 500 mg/L As(V)	2.60	-	29.8	-	67.6	44.8	-	73.5	-	530.0, 531.6
MA pH_{eq} 8 500 mg/L As(V)	0.700	-	30.5	-	68.8	44.5	-	73.6	-	530.5, 532.0
MA pH_{eq} 10 500 mg/L As(V)	0.600	-	29.5	-	70.0	44.5	-	73.6	-	530.2, 531.6
MA pH_{eq} 8 100 mg/L As(III)	-	0.600	31.2	-	68.2	-	43.3	73.4	-	529.9, 531.5
MA-5Fe	-	-	30.3	1.00	68.7	-	-	73.2	710.5	529.8, 531.3
MA-5Fe pH_{eq} 4 500 mg/L As(V)	2.50	-	28.4	1.00	68.2	44.7	-	73.2	710.6	529.7, 531.3
MA-5Fe pH_{eq} 8 500 mg/L As(V)	0.800	-	29.7	1.00	68.6	44.5	-	73.1	710.4	529.6, 531.2
MA-5Fe pH_{eq} 10 500 mg/L As(V)	0.600	-	28.7	1.10	69.5	44.7	-	73.5	710.7	530.0, 531.6
MA-5Fe pH_{eq} 8 100 mg/L As(III)	-	0.500	30.1	1.10	68.2	-	43.6	73.6	710.8	530.1, 531.7